

# Monitoring of Surface Deformation in Northern Taiwan Using DInSAR and PSInSAR Techniques

Chung-Pai Chang<sup>1,2,\*</sup>, Jiun-Yee Yen<sup>3</sup>, Andrew Hooper<sup>4</sup>, Fong-Min Chou<sup>1,2</sup>, Yi-An Chen<sup>5</sup>,  
Chin-Shyong Hou<sup>6</sup>, Wei-Chia Hung<sup>7</sup>, and Ming-Sheng Lin<sup>5</sup>

<sup>1</sup>Center for Space and Remote Sensing Research, National Central University, Zhongli, Taiwan, ROC

<sup>2</sup>Institute of Geophysics, National Central University, Zhongli, Taiwan, ROC

<sup>3</sup>Institute of Earth Sciences, National Hualien University of Education, Hualien, Taiwan, ROC

<sup>4</sup>Nordic Volcanological Center, University of Iceland, Reykjavik, Iceland

<sup>5</sup>Institute of Natural Science, Taipei Municipal University of Education, Taipei, Taiwan, ROC

<sup>6</sup>Central Geological Survey, MOEA, Taipei, Taiwan, ROC

<sup>7</sup>Energy and Resource Laboratories, Industrial Technology Research Institute, Hsinchu, Taiwan, ROC

Received 12 August 2008, accepted 20 November 2009

---

## ABSTRACT

We investigated the surface deformation of the northern Taiwan area, including the Taipei basin and its surrounding mountainous areas of the last fifteen years using the ERS-1, ERS-2 and ENVISAT SAR images. Although the Taipei basin now is well developed and amenable to research gathering using the Differential Interferometric Synthetic Aperture Radar (DInSAR) technique, the mountainous areas surrounding the basin are densely covered with various vegetation throughout different seasons inducing high noise ratio in interferograms. Therefore the DInSAR technique is ineffective for observation of surface deformations of these areas. As a result, we developed the Persistent Scatterer (PS) InSAR technique to extract the phase signal of the chosen PS points for this study. Our analysis result shows that the atmospheric disturbance and DEM residual can be successfully reduced and the precise information of surface deformation can be effectively obtained by the PSInSAR technique not only in the basin but also in the mountainous areas. Integrating the DInSAR and PSInSAR results, we observed conspicuous deformation events in northern Taiwan including: (1) the slight uplift in the Western Foothills, the Tatun volcanoes, the Linkou Tableland and the Taoyuan area; (2) the subsidence at the border of the Taipei basin; and (3) relative slight uplift rebound in the center of Taipei basin. The displacements along the Shanchiao, Chinshan, and Kanchiao Faults are large enough to be observed; the Taipei, Hsinchuang, and Nankang Faults are too small and cannot be discerned. Further comparison between the DInSAR, PSInSAR, and their corresponding leveling data shows a very coincidental pattern and measurably improves the authenticity of radar interferometry.

Key words: DInSAR, PSInSAR, ERS, ENVISAT, Surface deformation, Taipei basin, Northern Taiwan

Citation: Chang, C. P., J. Y. Yen, A. Hooper, F. M. Chou, Y. A. Chen, C. S. Hou, W. C. Hung, and M. S. Lin, 2010: Monitoring of surface deformation in northern Taiwan using DInSAR and PSInSAR techniques. *Terr. Atmos. Ocean. Sci.*, 21, 447-461, doi: 10.3319/TAO.2009.11.20.01(TH)

---

## 1. INTRODUCTION

Taiwan is located between the southeastern periphery of the Eurasian plate and the Philippine Sea plate. These two converging plates produced very active tectonics, which is revealed by the high seismicity and high deformation rate (for example, Ho 1986; Tsai 1986; Yu et al. 1997). Taipei, the most densely populated area, center of politics and

economics in Taiwan, is located in the Taipei basin at the northern part of the island. North of the Taipei basin, the Tatun volcanoes are assumed to be products of extensional collapse during the Pleistocene (Fig. 1; Teng 1990) after the collision between the Luzon volcanic arc and Eurasian continental margin at about 5 Ma (Figs. 1a and b). In the 1990s, the Unzen volcano on the island of Kyushu in Japan and the Mount Pinatubo of the middle Luzon Island erupted (for example, Bautista 1996; Newhall et al. 1996; Spence et al. 1996; Nakada et al. 1999; Yamashina and Shimizu 1999).

---

\* Corresponding author  
E-mail: cpchang@csr.ncu.edu.tw

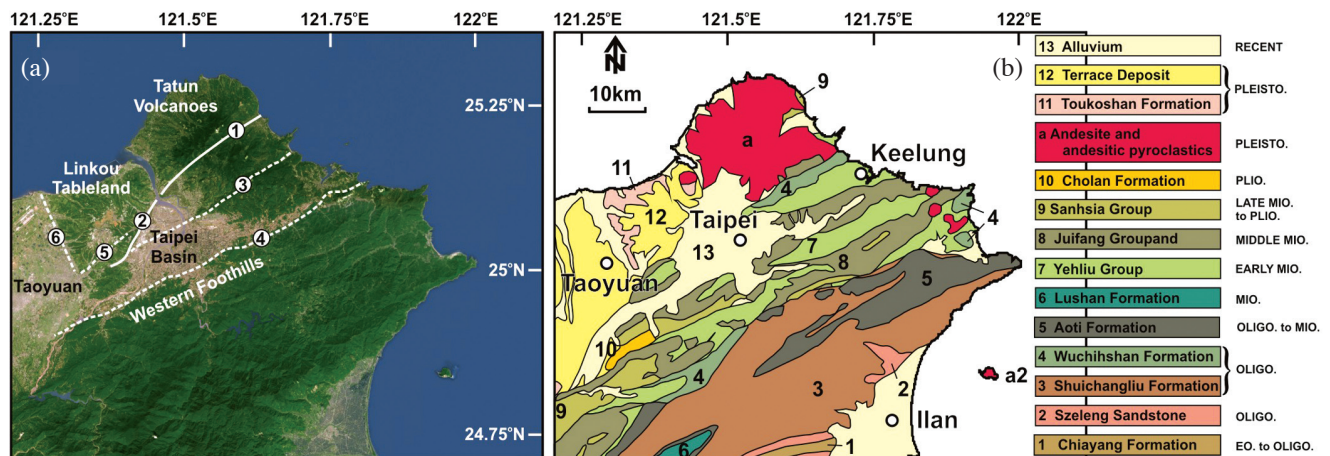


Fig. 1. (a) Morphology of the Northern Taiwan area. Shaded picture from SPOT satellite imagery (data from Center for Space and Remote Sensing Research Center, National Central University, 2006). The Taipei basin is nearly triangular in shape and is bordered by the Western Foothills to the south and east, the Tatum volcanoes to the north, and the Linkou Tableland to the west. Some fault lines marked by black lines include: (1) the Chinshan Fault; (2) Shanchiao Fault; (3) Kanchiao Fault; (4) Taipei Fault; (5) Hsinchuang Fault; and (6) Nankang Fault. After the Central Geological Survey's report (Lin et al. 2000) only the Chinshan and Shanchiao are active faults (in solid white line). (b) Generalised geology of the northern Taiwan area. Adapted from the Geological Map of Taiwan (published by the Central Geological Survey) and other maps.

Whether or not, like Unzen and Mount Pinatubo, the Tatum volcanoes might erupt is an issue that needs to be discussed. Moreover, several faults in and around the basin have been reported (Fig. 1). In order to understand the tectonic activity and mitigate the potential geological hazards of Taipei basin, monitoring the surface deformation in and around this basin should be a top priority.

In the past few years, Differential Interferometric Synthetic Aperture Radar (DInSAR) has proved to be a powerful technique for monitoring neotectonic activities and natural hazards (see, for example, Zebker et al. 1994; Massonnet and Feigl 1998; Chang et al. 2004). High spatial sampling rate of DInSAR technique allows studies of surface deformations with sub-centimeter accuracy. The aim of our study is to apply the space-borne DInSAR to determine the surface deformation of Taipei basin area, and discuss the relation between the deformation pattern and the surrounding faults. Therefore we chose 18 ERS-1 and ERS-2 SAR images acquired from 1993 to 2005 to generate 10 differential interferograms of the northern Taiwan area. Mountainous areas surrounding the Taipei basin are covered with various blooming vegetation over different seasons (see Fig. 1a). This induces a high noise ratio in interferograms and largely reduces the DInSAR technique's efficiency. As a result, in this study we applied the newly developed Persistent Scatterer (PS) InSAR technique in determining the surface deformation. The process details and results of these two techniques will be addressed in the following sections. Note that although the radar interferometry can be utilized as an effective geodetic tool with high spatial sampling density ( $\sim 100$  pixel  $\text{km}^2$ ), competitive precision ( $< 1$  cm), and useful observation cadence ( $\sim 1$  pass  $\text{month}^{-1}$ ), the radar im-

ages provide only the relative slant range change from the satellite view angle. Radar interferometric results cannot be considered as the real surface deformation and need to be compared to other geodetic measurements such as the GPS and precise leveling data to obtain more complete understanding of the regional deformation.

## 2. DIFFERENTIAL INTERFEROMETRY

### 2.1 Methodology and Data Acquisition

In order to detect surface deformation, first we applied the DInSAR technique. This approach extracts surface information by using the phase content of the radar signal as an additional information source derived from the complex radar data. Because of its great potential for mapping the movement associated with large earthquakes, the use of InSAR for monitoring earth deformation process has received considerable attention (see, for example, Zebker et al. 1994; Massonnet and Feigl 1998; Pathier et al. 2003; Chang et al. 2004). In northern Taiwan, the tectonic activity of our study area is relatively small and cannot be easily determined. However, for flat and well developed areas, such as the Taipei basin occupying the central part of the study area (Fig. 1), because of sensitive characteristic, the DInSAR technique is expected to reveal slight deformation features.

In this study, all used images are acquired from European Space Agency ERS-1 and ERS-2 satellites. The differential interferograms processing was done by applying DIAPASON software using a two-pass approach. The Taiwanese digital elevation model (DEM of Taiwan Forestry Bureau), which is retrieved from 1 : 5000 topographic maps and has a grid spacing of 40 m and average elevation accu-

racy of 1 m, was used to correct the topographic contribution. The detail processing procedure is shown in Fig. 2.

The phase difference between two radar images acquired at different times creates an interference pattern called an interferogram (Massonnet and Feigl 1998). Sensors loaded on ERS-1 and ERS-2 are C-band radars. Therefore each cycle in rainbow colors (one total phase change) in the resulted interferogram from red to blue, represents decrease (or increase) of 28 mm in length at the distance satellite versus earth surface. To clearly present our results, we proceeded the interferogram unwrapping by using the SNAPHU software (Fig. 2). For deformations reaching over 28 mm, after this unwrapping process, we can obtain the slant (radar line-of-sight) range displacement results.

All images used in this study belong to the scene of descending track 461/frame 3105 of ERS-1 and 2 satellites. To

generate 10 differential interferograms, we chose 18 images from 10 November 1993 to 30 April 2005, of which all perpendicular baselines are less than 100 m (Table 1 and Fig. 3). The short baseline provides good altitude for ambiguities, thus the phase contribution from orbital uncertainty in our interferograms is very small. Since the satellites on each pass do not exactly repeat same orbit, each successive image sample is a slightly different region of the Earth's surface. In order to compare the same region for deformation analysis, the images must be matched by aligning them to one reference image (or "master image", see Table 1). We used the precise orbit released by Delft Institute for Earth-Oriented Space Research (DEOS), along with an algorithm that compares the amplitudes of the pixels in two images, to evaluate shift and stretch parameters and then applied them to the repeated slave images. Its precision is better than 5 cm. It, hence, can theoretically avoid most errors caused by the orbit (Chang et al. 2004).

## 2.2 Analysis Results

The interferograms of each image pairs are shown in Fig. 4. The results show that a slight deformation in Taipei basin can be faintly observed. However, it seems to change through time. This may be caused by both the different deformation behaviors and the technical uncertainty. In fact, there are many factors that could affect the result of interferometry; in addition, the orbital error mentioned before and the non-stationarity error can also be distinguished. Non-stationarity errors are identified by two types. The first type is similar to the noise with a vibration within a limited range: for example, errors from DEM, residual errors caused by master and slave images, and errors caused by ground targets. The second type of non-stationarity error is similar to ground surface deformation. Distribution of this type of error is not related to the characteristics of ground targets. Instead, it is generally related to atmospheric conditions. Although radio wave can penetrate clouds and water vapor in the atmosphere, it attenuates during the penetration. In some cases, this kind of error can reach or even surpass 0.4 of a fringe in an interferogram (Pathier 2003). Moreover, this kind of error is not easy to be recognized in the interferometric result, and often brings the largest limitation to DInSAR measurement.

In this study, in order to restrain possible error, we pressed the observation cadence to its limit. As a result, from the winter of 1993 to the summer of 2005, all image pairs with a suitable baseline condition (less than 100 m) were chosen (Table 1; Fig. 3). The interferometric results of all image pairs are shown in Fig. 4. Because interferograms record only relative phase changes, we cannot identify the fringe corresponding to no deformation directly. Therefore we designated a point with a stable reflecting signal in all interferograms (in the center of the Taipei Basin) to carry out

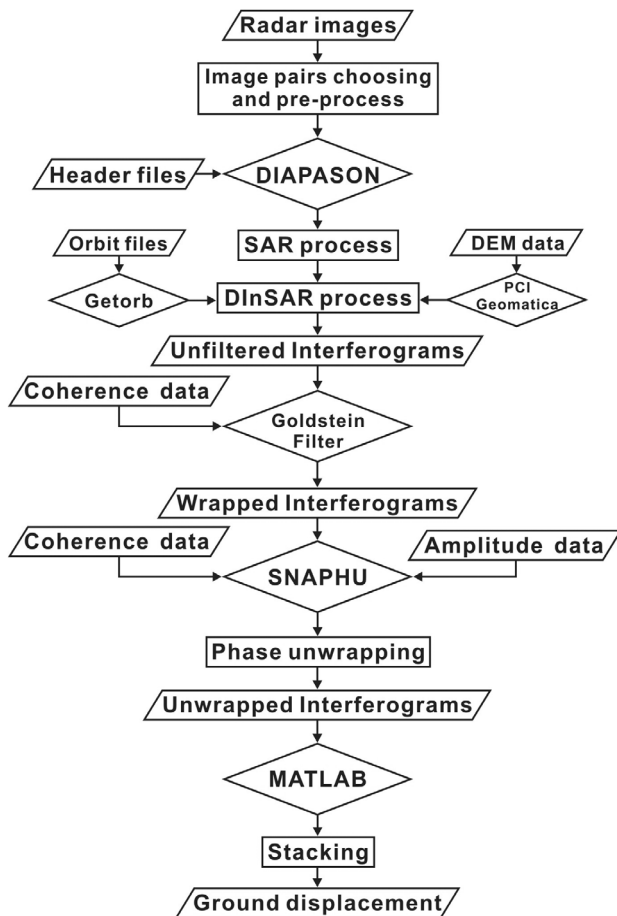


Fig. 2. Processing flowchart for DInSAR analysis used in this study. The main processes include: Raw data process, SAR image process, differential interferometry process, image filter process, phase unwrapping, stacking process. The SAR image and differential interferometry process were done by DIAPASON software by using the two-pass approach; and, the Taiwanese digital elevation model and precise orbital models released by Delft Institute for Earth-Oriented Space Research (DEOS) have been applied to correct for the topographic contribution.

an unwrapping operation and then stacked all unwrapped interferograms to obtain an average slant range displacement field of the study area (Fig. 5a). The mountainous area with low signal coherence has been masked in this stacked map. Note, the reference point in this study is man-designated; the deformation field shows the relative but not absolute value.

In case the cross-track displacement is limited, shortening in satellite slant range direction principally represents the land uplift and elongation can be considered as land subsidence. Inside the Taipei basin, because the relative horizontal displacement is very small (Rau et al. 2008), the slant range displacement pattern shown in Fig. 5a implies that the center of the Taipei basin is uplifted (rate in negative with warm colors); and the margin of the basin is relatively subsided (rate in positive with cold colors). The activity of the Shanchiao, Kanchiao and Taipei Faults appears to be insignificant for the deformation inside the basin.

Further, we compared our DInSAR result with precise leveling measurements from 1992 to 2003 achieved by Energy and Environment Research Laboratories, Industrial Technology Research Institute (ITRI annual report, 2001 ~ 2005). In general, to achieve a meaningful comparison, the displacement vector (in three components) measured by other technique needs to be projected onto the satellite slant range direction (Chang et al. 2004). However, in this study our comparisons are engaged without any projection processes and additional calculations. The reasons include (1) the leveling data only has a vertical component; (2) the incident angle is small (around 23°); and (3) the relative horizontal displacement in cross-track direction is very small (Rau et al. 2008). Figure 5b shows that the DInSAR result is

very consistent with the leveling measurement. Both clearly show that the largest subsidence occurred in western part (near point 2) and a relative uplift in central part of the basin (between point 5 to point 8).

Considering the irregularly distributed deformation pattern, ground water is a possible factor for recent deformation in the Taipei basin. According to some previous studies and local reports, for example Chen et al. (2007) and the Water Resources Agency's annual report, 1957 to 1973, a 40 meter water table decline has been observed causing at least 2 m of land subsidence. Also from 1974, the descending trend slowed down; from 1981, land subsidence was almost ceased; and since 1990, some local uplift events were reported however very small. Because the radar image dates back only to 1993, we cannot observe this change in the Taipei basin. Nevertheless, a slight uplift follow-up can still be observed in Fig. 5.

### 3. PERSISTENT SCATTERER INTERFEROMETRY

#### 3.1 Methodology and Data Acquisition

The DInSAR technique provides continuous observation for the flat area. However, for the mountainous area around the Taipei basin, because of the low correlation, this technique is unable to determine the phase change signal upon which to draw any conclusions about the regional surface deformation. For a SAR image, the value of each pixel remains the coherent sum of the returns from many scatterers on the ground. If these scatterers move or change with respect to each other along with time (between satellite passes), like scatterers of the vegetation or agriculture area, the returned phase will vary in a random manner which

Table 1. Parameters of SAR image pairs used for DInSAR analysis. Date of acquisition, interval time, and perpendicular baseline ( $B_{\perp}$ ) are shown. Track = 461, frame = 3105.

Pair	Master image	Satellite	Slave image	Satellite	$B_{\perp}$ (m)	Days
1	19950616	ERS-1	19931110	ERS-1	-24	583
2	19951208	ERS-1	19950721	ERS-1	-32	140
3	19970201	ERS-2	19951209	ERS-2	-57	420
4	19980328	ERS-2	19970308	ERS-2	-31	385
5	19990626	ERS-2	19970201	ERS-2	-55	875
6	19990904	ERS-2	19981024	ERS-2	54	315
7	20001028	ERS-2	20000122	ERS-2	-49	280
8	20010106	ERS-2	19990904	ERS-2	86	490
9	20041106	ERS-2	20030705	ERS-2	16	490
10	20050430	ERS-2	20030913	ERS-2	-78	595

leads to decorrelation. However, if a pixel is dominated by only one stable scatterer that is brighter than the background scatterers, the variance in the phase of the returning signal due to the change of the background scatterers will be re-

duced, and may be small enough for extracting the underlying deformation signal. Ferretti et al. (2000 and 2001) first identified this type of pixel as a Permanent Scatterer™. In order to avoid this trademarked name, now we generally

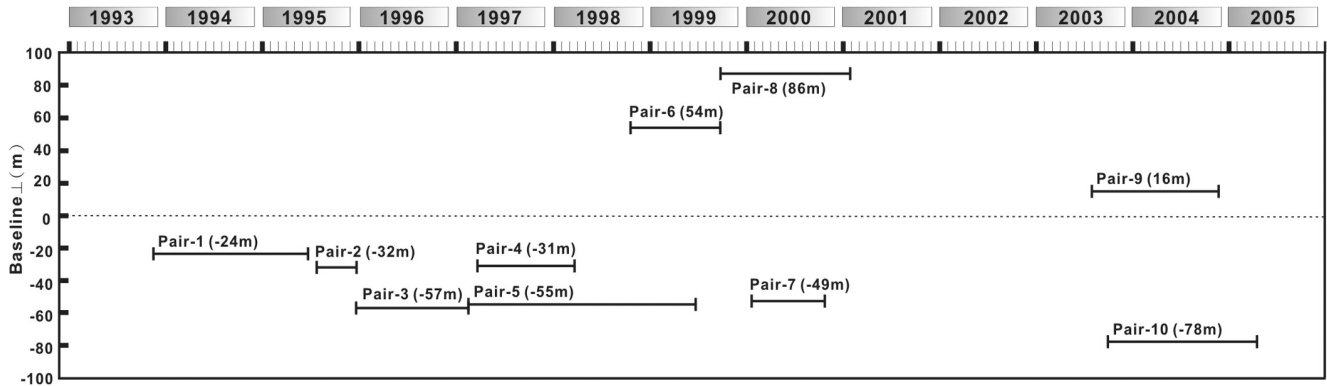


Fig. 3. Image pairs used for DInSAR analysis in this study. All images are acquired by satellites ERS-1 and 2 in the descending orbit track 461, frame 3105. Cross axle: acquisition time; vertical axle and the number in parentheses: perpendicular baseline ( $B_{\perp}$ ) in meter.

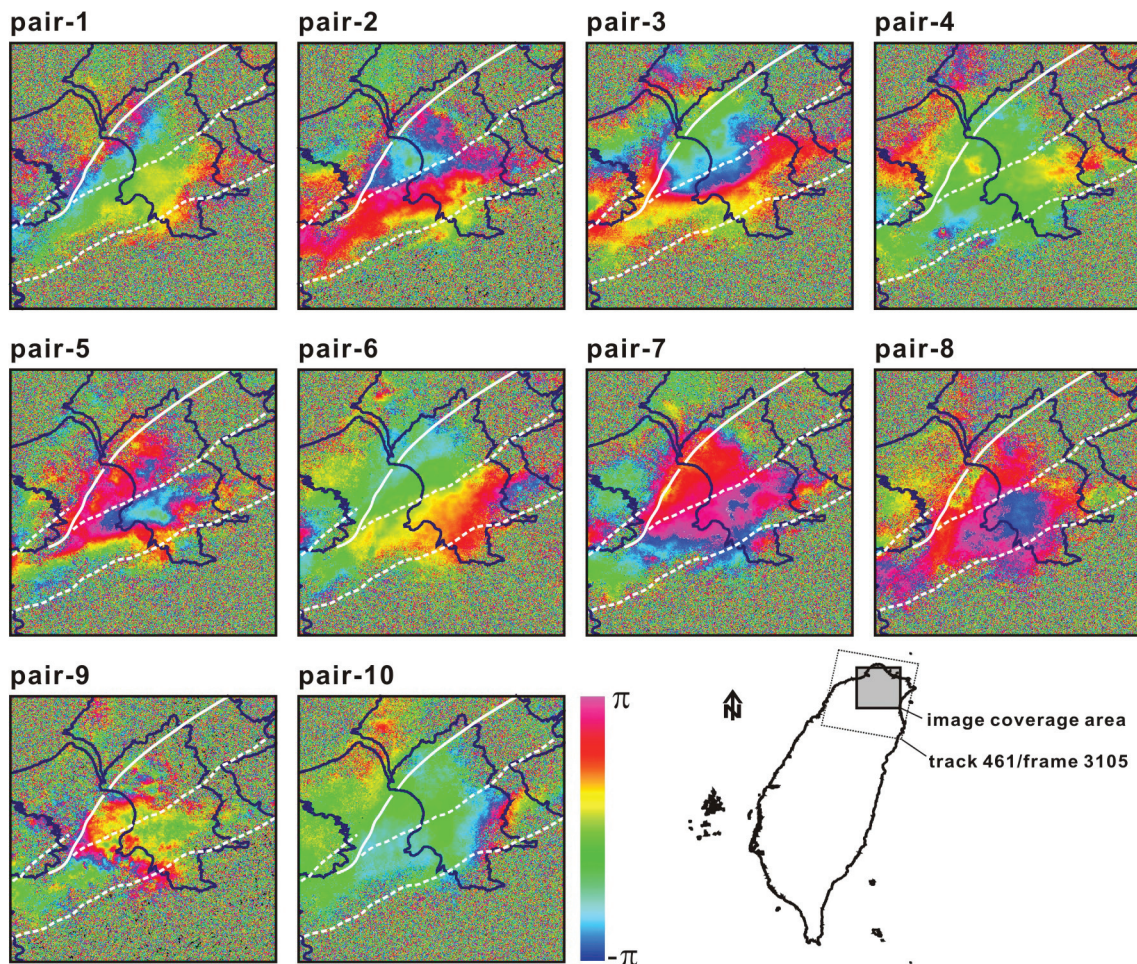


Fig. 4. Differential interferograms of the northern Taiwan area. Time interval and perpendicular baseline are shown in Fig. 3 and Table 1. White line: fault line; blue line: administrative boundary.

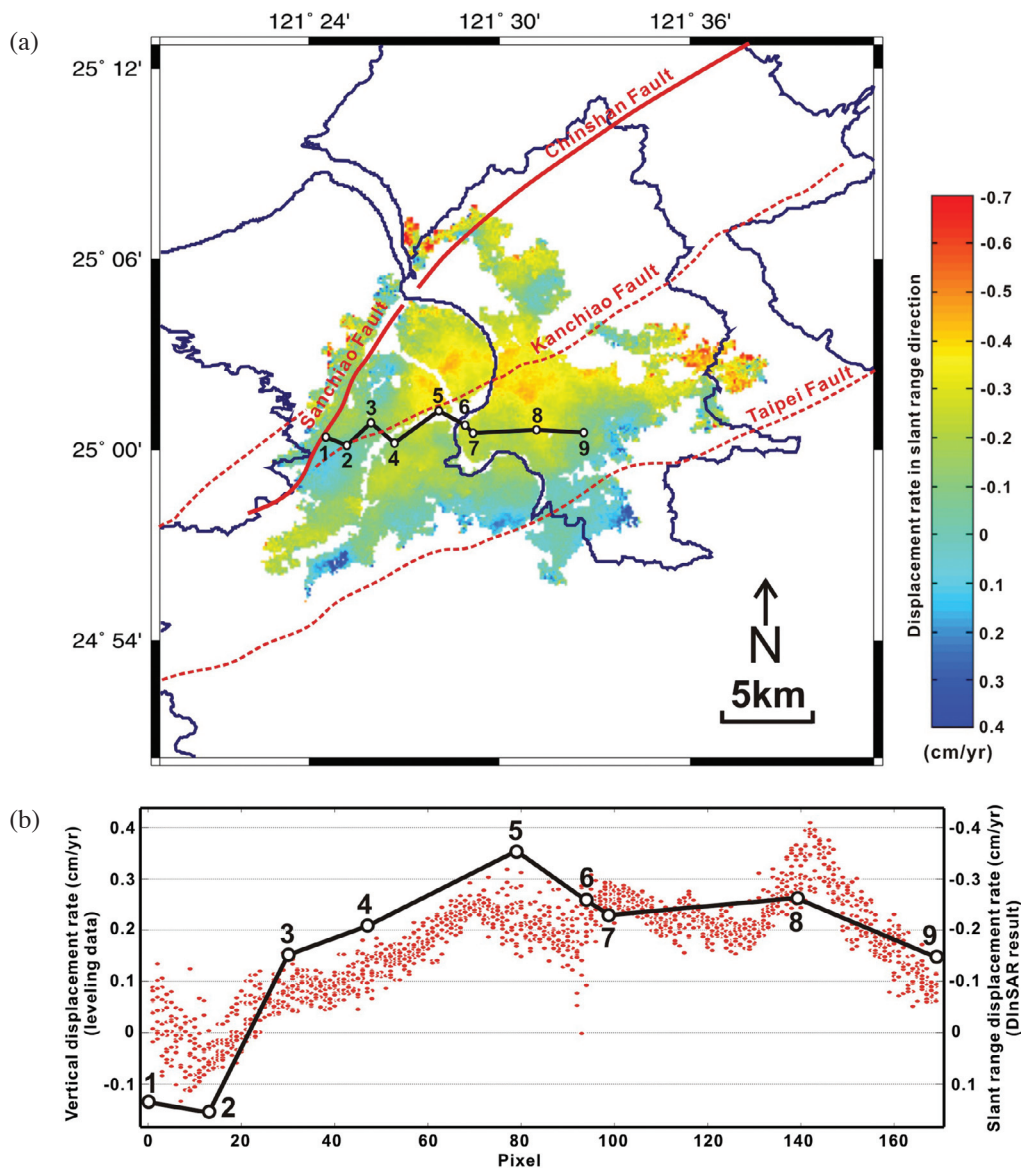


Fig. 5. (a) Stacked unwrapped result of the interferograms in Fig. 4. Red line: fault line; blue line: administrative boundary; points 1 ~ 9: leveling survey points of Energy and Environment Research Laboratories, Industrial Technology Research Institute. (b) Comparison between leveling measurement (white points linked by black line) achieved from 1992 to 2003 by ITRI (ITRI annual report, 2001 ~ 2005) and DInSAR result (small red points) based on images acquired from 1993 to 2005.

use persistent scatterer to call this type of pixel. Physically, these stable scatterers might be a tree trunk or a single large rock among the vegetation.

Methods to identify and isolate these PS pixels in interferograms have been developed by several groups (e.g., Ferretti et al. 2001; Adam et al. 2003; Crosetto et al. 2003; Lyons and Snadwell 2003; Werner et al. 2003; Kampes 2005). All of these methods use a functional model of how deformation varies with time to figure PS pixels, and have been very successful in calculating PS pixels in urban areas undergoing (primarily) steady state or periodic deformation. In these algorithms, initial set of PS pixels with a high signal-to-noise ratio is identified by analyzing the amplitude

variation, pixel by pixel, in a series of interferograms. Once an initial set of amplitude-stable pixels has been identified, each candidate pixel is tested for phase stability by examining its phase differences with nearby candidates. This approach can fail for two reasons. First, it can fail if the distance between neighboring PS pixels is too large, such that the contribution to the unmodeled phase from the difference in delay along the raypaths through the atmosphere exceeds the limit for reliable unwrapping. The second limitation is that an approximate model for the temporal variation in deformation is needed to isolate the deformation signal from atmospheric, topographic and other phase errors. As the time dependence of deformation is not usually known *a*

*priori*, it is usually assumed to be approximately constant in rate or periodic in nature.

Hooper et al. (2004 and 2007) developed a new PS method to extract the deformation signal from SAR data of the area that contains few man-made structures and that deformed at variable rates during the time interval analysis. This method largely increases the accuracy of the estimated displacements and also makes it applicable in area with widely varying deformation gradients. In this study, we apply Hopper's method, the StaMPS (Stanford Method for PS, Hooper et al. 2007), for identifying PS pixels and estimating their displacement. The detail processing procedure is shown in Fig. 6. All images used in this study are acquired by descending European Space Agency ENVISAT satellite. In all, we chose 21 images from 22 November 2003 to 1 December 2007 to calculate the displacement field of the northern Taiwan area (Table 2; Fig. 7). Considering the baseline condition and time span, the master image is fixed on 17 September 2005. The maximum perpendicular baseline is 824 m.

### 3.2 Analysis Results

Figure 8 shows the unwrapped phase of PS pixels of each image referenced to the master image. In these interferograms the Taiwanese digital elevation model mentioned

before has been applied to remove the topographic effect; however, the residual phase results shown in Fig. 8 still contain errors from several other sources. Theoretically, the residual phase,  $\phi$ , of the  $x$ th pixel in the  $i$ th topographically corrected interferogram can be written as the sum of 5 terms,

$$\phi_{x,i} = \phi_{def,x,i} + \phi_{\alpha,x,i} + \phi_{orb,x,i} + \phi_{\epsilon,x,i} + n_{x,i} \quad (1)$$

where  $\phi_{def}$  is the phase change due to movement of the pixel in the satellite line-of-sight (LOS) direction,  $\phi_{\alpha}$  is the phase equivalent of the difference in atmospheric retardation between passes,  $\phi_{orb}$  is the phase due to orbit inaccuracies,  $\phi_{\epsilon}$  is the residual topographic phase due to error in the DEM and  $n$  is the noise term due to variability in scattering from the pixel, thermal noise and coregistration errors. Because the PS pixels were defined where  $n$  is small enough, this component will not be discussed below.

The phase error from uncertainty in the DEM is proportional to the perpendicular component of the baseline,  $B_{\perp}$ ; this error can thus be estimated and corrected by using precise orbit data (Hooper et al. 2004) (Fig. 9a). After correction for estimated DEM error, the phase difference between neighboring PS is generally less than  $\pi$ , the corrected phase values can thus be unwrapped. After unwrapping, the atmospheric and orbit errors still remain in interferograms

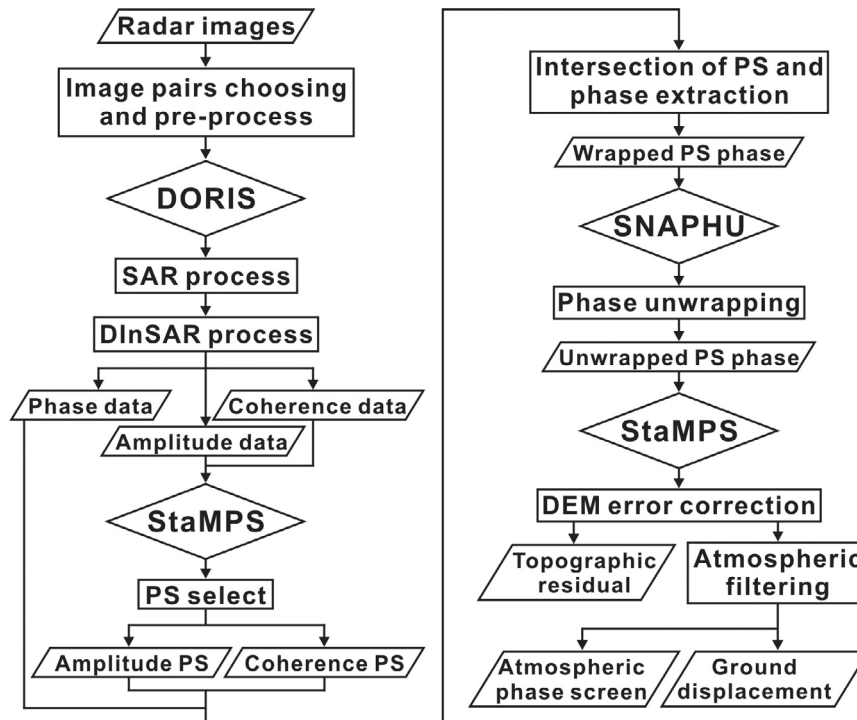


Fig. 6. Processing flowchart for PSInSAR analysis used in this study. The main processes include: Raw data process, SAR image process, differential interferometry process, PS selecting, intersection of PS and phase extracting, phase unwrapping, DEM error correcting, atmospheric filtering. The SAR image and differential interferometry process were done by DORIS software, all PS processes were done by StaMPS software developed by Hooper et al. (2004).

Table 2. Parameters of ENVISAT-SAR images used for PSInSAR analysis. The master image is fixed on 17 September 2005. 2004 Information of the slave images of each pair, including date of acquisition, interval time, and perpendicular baseline ( $B_{\perp}$ ) with the master image are shown. Track = 461, frame = 3105.

Pair	Satellite	Date	Orbit	$B_{\perp}$ (m)	Days
1	ENVISAT	20031122	9032	-824.6	-665
2	ENVISAT	20040306	10535	-270	-560
3	ENVISAT	20040410	11036	476.8	-525
4	ENVISAT	20040515	11537	-538.6	-490
5	ENVISAT	20040619	12038	-224.2	-455
6	ENVISAT	20040724	12539	77.7	-420
7	ENVISAT	20040828	13040	-261.5	-385
8	ENVISAT	20041002	13541	-324.7	-350
9	ENVISAT	20041106	14042	-250.4	-315
10	ENVISAT	20041211	14543	-458.5	-280
11	ENVISAT	20050604	17048	-609.9	-105
12	ENVISAT	20050709	17549	617.3	-70
13	ENVISAT	20050813	18050	-628.9	-35
Master Image	ENVISAT	20050917	18551	0	0
14	ENVISAT	20060902	23561	206.4	350
15	ENVISAT	20061007	24062	-735.8	385
16	ENVISAT	20070120	25565	164.2	490
17	ENVISAT	20070224	26066	-126.6	525
18	ENVISAT	20070331	26567	78.9	560
19	ENVISAT	20070714	28070	-306	665
20	ENVISAT	20071201	30074	-101.8	805

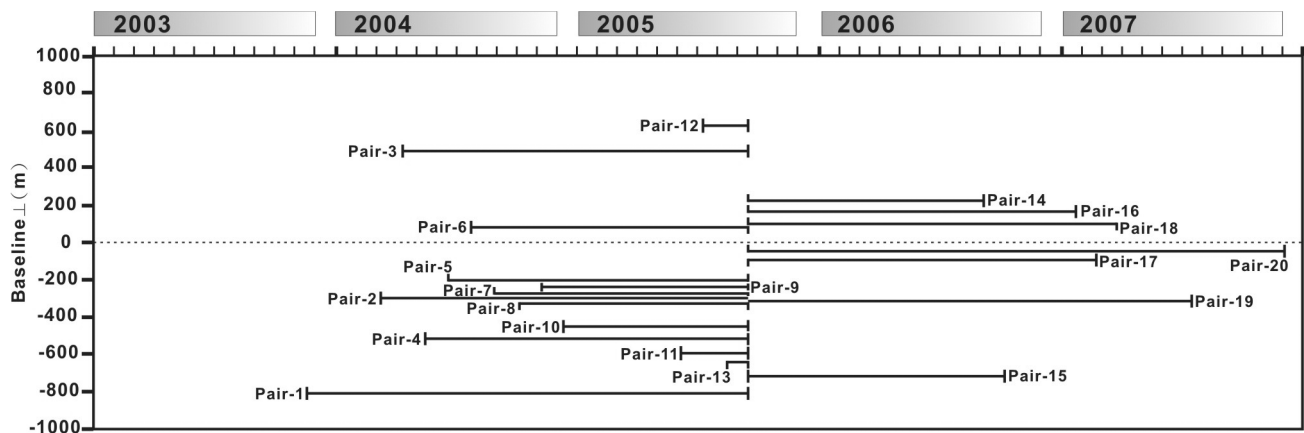


Fig. 7. Image pairs used for PSInSAR analysis in this study. All images are acquired by satellite ENVISAT in the descending orbit track 461, frame 3105. Cross axle: acquisition time; vertical axle and the number in parentheses: perpendicular baseline ( $B_{\perp}$ ) in meter. Considering the baseline condition and time span, the master image is fixed on 17 September 2005. The maximum perpendicular baseline is 824 m of pair-1. Some detail parameters in Table 2.

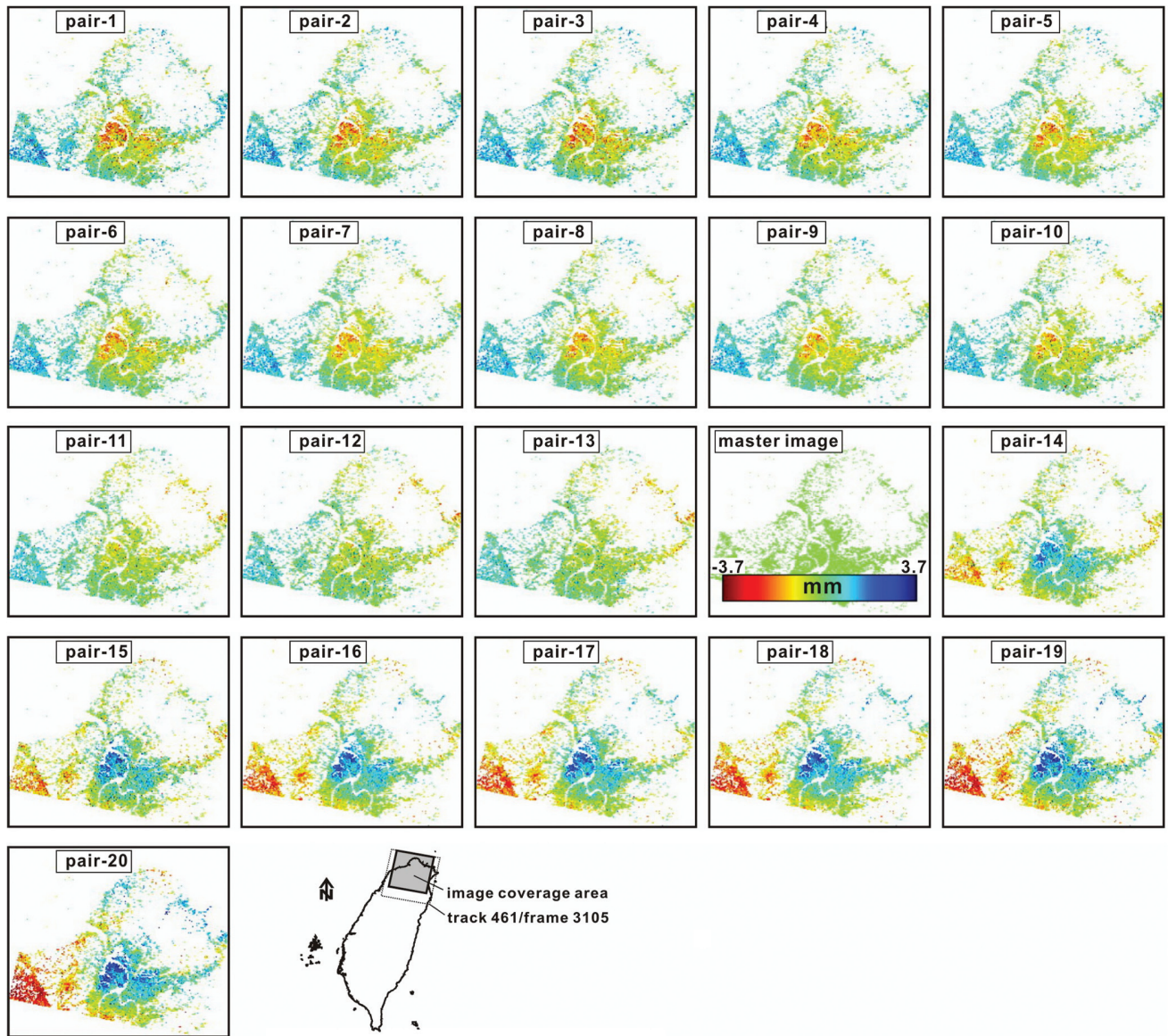


Fig. 8. Unwrapped phase of PS pixels of each images referenced to the master image. Time interval and perpendicular baseline are shown in Fig. 7.

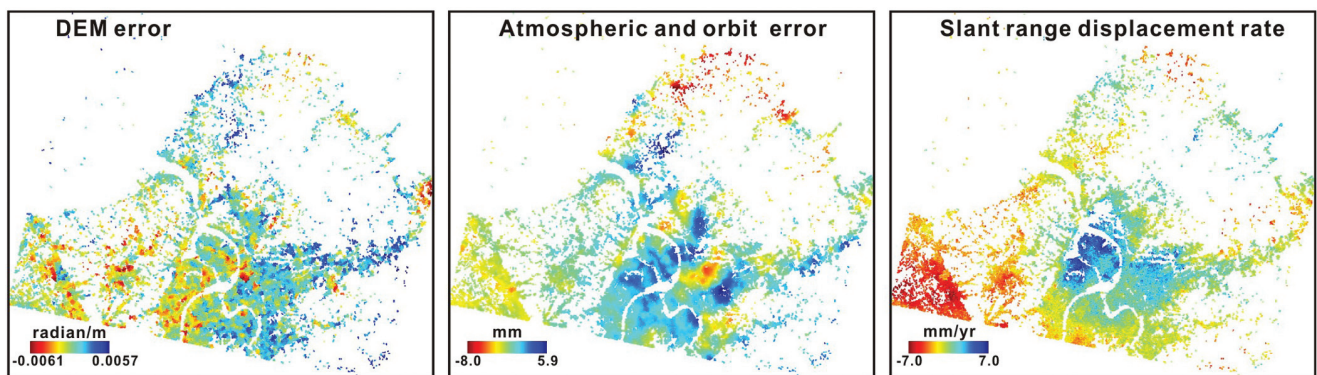


Fig. 9. (a) Estimated DEM error of master image. (b) Atmospheric and orbit error of master image. (c) The unwrapped residual phase result of PS pixels. Because the errors of (a) and (b) have been removed, this result can be considered as the slant range displacement rate between the PS and satellite.

and mask  $\phi_{def}$ . Unlike  $\phi_{def}$ , the spatially correlated portion of these terms is assumed to be uncorrelated temporally. Thus, by high-pass filtering the unwrapped data in time then low-pass filtering in space we are able to estimate the spatially correlated error (Ferretti et al. 2001) (Fig. 9b). Subtracting this signal from interferograms leaves just  $\phi_{def}$  and spatially uncorrelated error terms that can be modeled as noise.

Figure 9c shows the unwrapped residual phase result of PS pixels, in which the errors mentioned before have been removed. Therefore it can reflect the line-of-sight distance change rate between the PS and satellite. With the same definition in color, in this figure shortening (rate in negative value with warm colors) represents land uplift and elongation (rate in positive value with cold colors) represents land subsidence in a slant range direction. Because the PSInSAR provides only the relative observation, the results shown in Fig. 9c are not the absolute displacement rate but only the relative offset with neighboring areas. For example, the apparent subsidence in Taipei basin just suggests that the relative offset between the Linkou Tableland and the Taipei ba-

sin reaches about  $10 \text{ mm yr}^{-1}$  for the observing time span.

In order to obtain a reasonable displacement field and conveniently compare other measurements, we used the base point of “Taiwan Vertical Datum 2001” (known as TWVD 2001) installed by the Department of Land Administration, Ministry of the Interior in Keelung harbor as the control point (fixed pixel) to adjust our PS result (Fig. 10). After this adjustment, the slant range pattern shown in Fig. 10 can be considered as the phase result of near-true surface deformation. The most conspicuous pattern is the subsidence inside the Taipei basin. Still, some uplifts (shortening in slant range direction) can also be observed in the Linkou Tableland, the Western Foothills, the Tatun volcanoes, and in the mountainous area between the Kanchiao and Taipei Faults (Fig. 10). The vertical displacement rate obtained by a recent leveling survey (2004 ~ 2005 and 2005 ~ 2006) along the Tanshui River and the northern coastal line (Lines A and B in Fig. 10; Hou 2007) provides us a good opportunity to check our PSInSAR observation. As the same reason mentioned before, we engaged in this com-

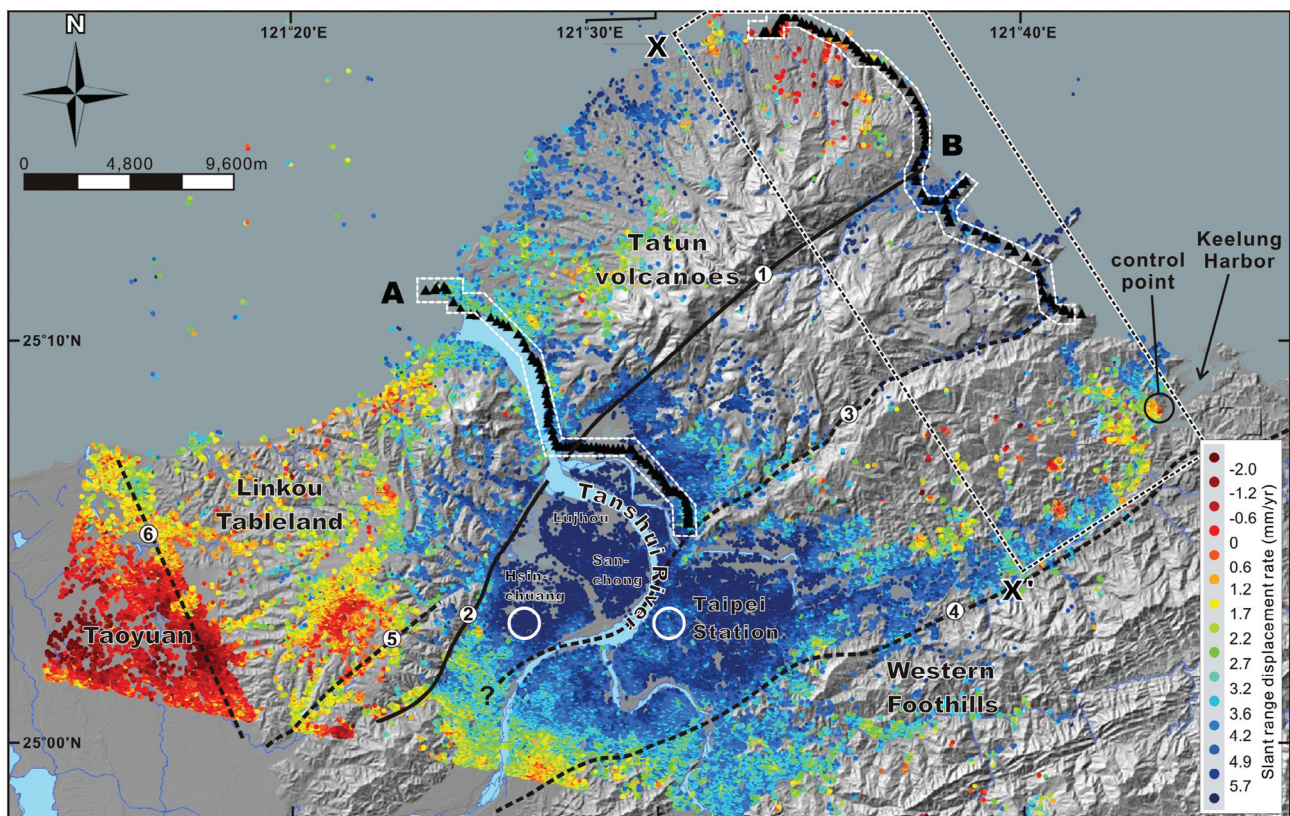


Fig. 10. Slant range displacement rate of the processed PSs in the northern Taiwan area. This result has been adjusted by using the base point of “Taiwan Vertical Datum 2001” installed by the Ministry of the Interior in Keelung harbor as the control point. Topographic map in background is the Taiwan digital elevation model from Taiwan Forestry Bureau. Shortening in slant range (rate in negative with warm colors) represents land uplift and elongation (rate in positive with cold colors) represents land subsidence in slant range direction. Black solid lines mark the main active faults and dashed lines are the inactive faults defined by the Central Geological Survey: (1) Chinshan Fault; (2) Shanchiao Fault; (3) Kanchiao Fault; (4) Taipei Fault; (5) Hsinchuang Fault; and (6) Nankang Fault. Black triangular: leveling survey points after Hou (2007). White dashed lines encircled the PS pixels that will compare with leveling data along profiles A and B in Fig. 11. Black dashed line frame XX’ defines the PS pixels that will show in Fig. 12.

parison without any projection processes. Figure 11 shows that along profiles A and B the PSInSAR results fit well with their corresponding leveling data; both show that the Chinshan Fault is a clear boundary, across which the displacement rate clearly demonstrates the difference (eastern side is relatively subsiding). This consistency largely enhances our confidence on PSInSAR technique and encourages us to derive the following discussion.

#### 4. DISCUSSION

The drilling data shows that the Taipei basin is flooded with Tertiary basement and filled with flat-lying Quaternary sediments. The depth of the basement increases from the

eastern margin toward its western margin, where it reaches the maximum depth of about 670 m (Wang et al. 1995; Teng et al. 2001). This configuration suggests that the Taipei basin may be a half-graben abutting against the Shanchiao Fault, which is an east-dipping high angle normal fault (Lin et al. 2000) in the western boundary of the Taipei basin. Under this configuration, the area near the Shanchiao Fault should have a higher subsidence rate. Even the trace of the Shanchiao Fault cannot be clearly observed, our PSInSAR result generally supports this expected pattern and shows that the largest subsidence rate occurred in the Lujhou, Hsinchuang, and Sanchong areas (Fig. 10).

Because the Tatun volcanoes were recently active, and at around 0.2 Ma a lahar derived from the Tatun volcanoes

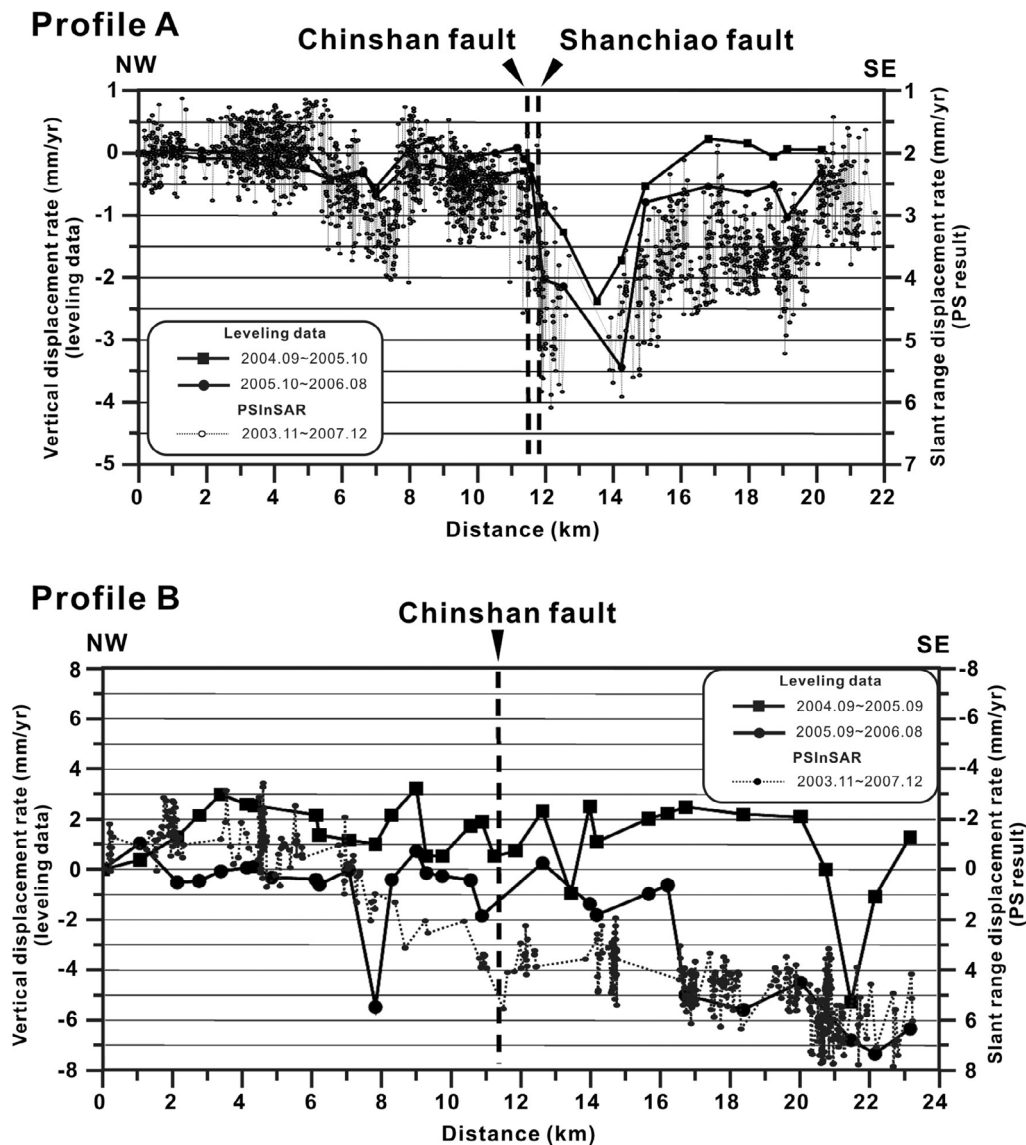


Fig. 11. Comparison between the leveling data (Hou 2007) and PSInSAR result along the northern coastal line (Profile A) and the northern bank of Tanshui River (Profile B). Leveling data are relative to the western most point of the profile; PS displacements are relative to the control point shown in Fig. 10. Locations of profiles in Fig. 10.

blocked the outlet of the Tanshui River inundating the Taipei basin and creating a lake (Teng et al. 1991). The active deformation of Tatun volcanoes and relative faults is an issue that should be discussed. In Fig. 10, the PS result shows a clear displacement pattern for the Tatun volcanoes area: considering the Chinshan Fault as a boundary, by comparing with the southeastern side, northwestern is under relative uplifting. Near the northern coastal area, this displacement is obvious, but it is very obscure in the central part of the Chinshan Fault where this fault is partially covered Pleistocene volcanic breccia (Lin et al. 2000) and is difficult to be traced. In the southern part of the Chinshan Fault, this displacement can be observed and connected with that of the Shanchiao Fault.

Also the average altitude of volcanoes on the northwestern side of the Chinshan Fault is higher than that on the southeastern side (Fig. 10). This topographic feature implies that the movement along Chinshan Fault is not a recent event but might have been active in a distant period. However, this observation does not follow the geometry and kinematics of the Chinshan Fault proposed in previous studies: as an east-dipping reverse fault (e.g., Lin et al. 2000). Our preliminary explanation is that the recent displacement occurring along the Chinshan Fault may be controlled by the post-collision extensional tectonic regime as proposed by Teng et al. (1991). This extensional tectonic regime reopened the relic of Chinshan Fault but in normal faulting manner (east-dipping high angle normal faulting). In the south, the activity along the Chinshan Fault can be related to the newly generated Shanchiao Fault, which plays an important role in forming the Taipei basin.

East of the Tatun volcanoes, activity of the Kanchiao

Fault can also be observed (Fig. 10). The PSs on southeastern side of Kanchiao Fault are relatively uplifted compared with those on the northwestern side (Figs. 10 and 12). The Kanchiao Fault has been reported as an east-dipping reverse fault by previous studies (for example Huang et al. 1991), the observed deformation pattern can thus be explained as an activity of this reverse fault. But, if we consider the regional tectonic regime and the movement of the Chinshan Fault mentioned before, this displacement along Kanchiao Fault could also be the result of west-dipping normal faulting. Some further evidence supporting the normal faulting mechanism includes: (1) the subsidence rate almost equal anywhere in the block between Chinshan and Kanchiao Faults without any tilting what often appears associated with a thrust faulting (Fig. 12); (2) the movement of the Tanshui River channel from the western border of the Taipei basin to its center, forming a good fit with the possible southern prolongation of Kanchiao Fault (see the abandoned river channel west to Lujhou and Sanchong in Fig. 10); (3) normal faulting type in most shallow earthquake focal mechanism solutions (Yeh 1990, unpublished report). All these features force us to believe that, even at the beginning its nature was reversed, the west-dipping normal faulting plays an important role in the recent movement along the site of Kanchiao Fault.

The deformation inside the Taipei basin can be observed by both DInSAR and PSInSAR techniques. In Fig. 5, the relative displacement field of DInSAR shows that the center of the Taipei basin is under uplifting and the margin of the basin is under subsidence. This pattern is not obvious in the PSInSAR result shown in Fig. 10 because of two reasons: (1) after an adjustment considering the base

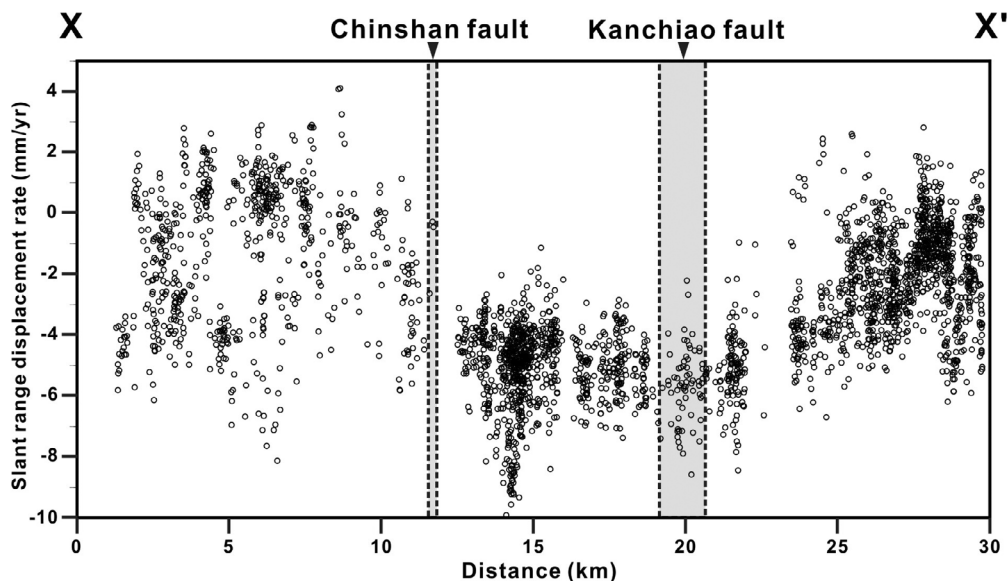


Fig. 12. Slant range displacement of PS pixels in the northern tip of Taiwan Island (in frame XX' of Fig. 10). Clear subsidence can be observed in the terrain between the Chinshan and Kanchiao Faults.

point of TWVD 2001 as the fixed pixel, the PS pixels inside the Taipei basin are all during the subsidence; (2) the time span for DInSAR (from the winter of 1993 to the summer of 2005) and PSInSAR (from the end of 2003 to the end of 2007) analyses are different. After some local reports and previous studies (e.g., Chen et al. 2007), the relative uplift rate in the center of Taipei basin slowed down after 2000 and may have even ceased in 2003. The difference pattern between DInSAR and PSInSAR results may just reflect this change. Because these two results fit well with their compared leveling data (for DInSAR, leveling data acquired from 1992 to 2003 and for PSInSAR, leveling data acquired from 2004 ~ 2006), we consider that the patterns in Figs. 5a and 10 are all acceptable. Anyhow, in PSInSAR result we can still observe that the central part of Taipei basin is under relative uplift. Comparing the Hsinchuang area, the uplift rate of the Taipei station is about  $2 \text{ mm yr}^{-1}$  (Fig. 10), which reaches almost a half of the rate determined by DInSAR technique shown in Fig. 5.

The deformation pattern of the Linkou Tableland and Taoyuan area shown in Fig. 10 is smoother. The relative displacement rate between the Linkou Tableland and the Taoyuan area is less than  $2 \text{ mm yr}^{-1}$  during the observing time span and does not reveal any clear relationship with the fault distribution. In that area, there are many large industrial parks with factories, which before 2000, pumped a considerable amount of the ground water for industrial use and induced large scale land subsidence in many places (Chang et al. 2004). Therefore, the uplifting pattern in this area may reflect a post-pumping rebound. To sum up, for the area west to the Shanchiao Fault, the surface deformation seems to be without any relationship with Hsinchuang and Nankang Faults. Thus we infer that these two faults may be inactive during our observing time span from 2003 to 2007.

## 5. CONCLUSION

In this study, DInSAR and PSInSAR techniques have been applied to observe the surface deformation of the northern Taiwan area. Each technique has its own strength and weakness. For example, the advantage of the DInSAR technique is that the surface deformation information can be directly extracted by using only two images acquired at different times; the weakness rests principally in the weather conditions, a different weather pattern of an image acquisition time may usually raise a considerable residual atmospheric error. Even though we can remove most atmospheric errors by stacking interferograms of different time spans (for example, the case shown in Fig. 5a), some atmospheric effects are believed to be still existed. Moreover, after stacking process, the displacement field that we obtained is a mathematical average displacement rate; some temporal and local events can be diluted and could not be revealed. The other limitation for the DInSAR technique is from the

topography and covered vegetation. Both of these reduce the coherence of radar images making phase analysis very difficult. It is why the result shown in Fig. 5a covers only the urbanized flat inside the Taipei basin.

Development of PSInSAR is aimed at solving the weakness of DInSAR. This technique considers only the stable scatterer that is brighter than the background scatterer and thus can reduce the noise ratio in radar image and effectively extract the deformation signal. Since PSInSAR technique does not use every scatterer on the ground, the resolution (density of pixels) of this technique in a mountainous area with dense vegetation can be consequently reduced; phase unwrapping in the PSInSAR technique is therefore a crucial process for the area with lower PS density. Another constraint for PSInSAR is data acquisition and observation time span. For an effective PS calculation, at least around twenty images are needed, the shortest observation time period, considering the observation cadence as 1 pass per 35 days, is at least 2 years. For the emergent and temporal event, such as the co-seismic surface deformation associated with large earthquake, the PSInSAR technique is thus difficult to apply.

The DInSAR technique successfully revealed the displacement pattern of the Taipei basin but failed in revealing a similar pattern to the surrounding mountainous area. In order to observe the deformation of mountainous area, we utilized the PSInSAR technique to engage this measurement. Our results proved that the PS technique is capable in measuring the deformation of mountainous areas; the deformations of Tatun volcanoes, Linkou Tableland and Western Foothills are all clearly exposed. In this study, we further compared the DInSAR and PSInSAR results with the corresponding leveling data. The coincidence between these techniques with different natures largely improved our confidence on radar interferometry. We conclude that the PS technique is capable of measuring a mountainous area with vegetation in subtropical areas such as Taiwan orogene. We believe that in the future, this technique will be usefully applied to other areas, especially for remotely and locally developed Western Foothills where is threatened by the active faults and geological hazards.

**Acknowledgements** We are deeply grateful to two anonymous reviewers for critical comments and wise suggestions on this paper. This work was supported by the National Science Council (grant No. NSC96-2119-M-008-013) of Taiwan. ENVISAT data was provided by ESA under the project of Earth Observation (contract No. EOPI-4427).

## REFERENCES

Adam, N., B. Kampes, M. Eineder, J. Worawattanamatekul, and M. Kircher, 2003: The development of a scientific permanent scatterer system. Paper presented

- as ISPRS Hannover Workshop, Inst. for Photogramm. and Geoinf., Hannover, Germany.
- Bautista, C. B., 1996: The Mount Pinatubo disaster and the people of Central Luzon. In: Newhall, C. G. and R. S. Punongbayan (Eds.), *Fire and Mud: Eruptions and Lahars of Mount Pinatubo*, University of Washington Press, Seattle, 151-164.
- Chang, C. P., C. T. Wang, T. Y. Chang, K. S. Chen, L. S. Liang, E. Pathier, and J. Angelier, 2004: Application of SAR interferometry to a large thrusting deformation: The 1999  $M_w = 7.6$  Chichi earthquake in Central Taiwan. *Geophys. J. Int.*, **159**, 9-16, doi: 10.1111/j.1365-246X.2004.02385.x. [[Link](#)]
- Chen, C. T., J. C. Hu, C. Y. Lu, J. C. Lee, and Y. C. Chan, 2007: Thirty-year land elevation change from subsidence to uplift following the termination of groundwater pumping and its geological implications in the Metropolitan Taipei Basin, Northern Taiwan. *Eng. Geol.*, **95**, 30-47, doi: 10.1016/j.enggeo.2007.09.001. [[Link](#)]
- Crossetto, M., A. Arnaud, J. Duro, E. Biescas, and M. Agudo, 2003: Deformation monitoring using remotely sensed radar interferometric data. Paper presented at 11th FIG Symposium on Deformation Measurements, Patras Univ., Santorini, Greece.
- Energy and Environment Research Laboratories, Industrial Technology Research Institute, 2001 ~ 2005 annual reports of project entitled "Land subsidence survey, investigation and analysis of Taiwan area", funded by Ministry of Economic Affairs.
- Ferretti, A., C. Prati, and F. Rocca, 2000: Nonlinear subsidence rate estimation using permanent scatterers in differential SAR interferometry. *IEEE Trans. Geosci. Remote Sensing*, **38**, 2202-2212, doi: 10.1109/36.868878. [[Link](#)]
- Ferretti, A., C. Prati, and F. Rocca, 2001: Permanent scatterers in SAR interferometry. *IEEE Trans. Geosci. Remote Sensing*, **39**, 8-20, doi: 10.1109/36.898661. [[Link](#)]
- Ho, C. S., 1986: A synthesis of the geologic evolution of Taiwan. *Tectonophysics*, **125**, 1-16, doi: 10.1016/0040-1951(86)90004-1. [[Link](#)]
- Hooper, A., H. Zebker, P. Segall, and B. Kampes, 2004: A new method for measuring deformation on volcanoes and other natural terrains using InSAR persistent scatterers. *Geophys. Res. Lett.*, **31**, L23611, doi: 10.1029/2004GL021737. [[Link](#)]
- Hooper, A., P. Segall, and H. Zebker, 2007: Persistent scatterer interferometric synthetic aperture radar for crustal deformation analysis, with application to Volcan Alcedo, Galapagos. *J. Geophys. Res.*, **112**, B07407, doi: 10.1029/2006JB004763. [[Link](#)]
- Hou, C. S., 2007: Monitoring of active structures related crustal deformation in Taiwan. Ph.D. Thesis, Institute of Geosciences, National Taiwan University, Taiwan, ROC.
- Huang, C. S., C. F. Lee, and H. C. Liu, 1991: The geological investigation of the Kanchiao Fault, northern Taiwan. *Bull. Cent. Geol. Surv.*, **7**, 23-42.
- Kampes, B. M., 2005: Displacement parameter estimation using permanent scatterer interferometry. Ph.D. Thesis, Delf University of Technology, Delf, Netherlands.
- Lin, C. W., H. C. Chang, S. T. Lu, T. S. Shih, and W. J. Huang, 2000: An introduction to the active faults of Taiwan. *Spec. Publ. Cent. Geol. Surv.*, **13**, 122 pp. (in Chinese)
- Lyons, S. and D. Sandwell, 2003: Fault creep along the southern San Andreas from interferometric synthetic aperture radar, permanent scatterers, and stacking. *J. Geophys. Res.*, **108**, B12047, doi: 10.1029/2002JB001831. [[Link](#)]
- Massonnet, D. and K. L. Feigl, 1998: Radar interferometry and its application to changes in the Earth's surface. *Rev. Geophys.*, **36**, 441-500.
- Nakada, S., H. Shimizu, and K. Ohta, 1999: Overview of the 1990-1995 eruption at Unzen volcano. *J. Volcanol. Geotherm. Res.*, **89**, 1-22, doi: 10.1016/S0377-0273(98)00118-8. [[Link](#)]
- Newhall, C., A. Daag, F. D. Delfin Jr., R. Hoblitt, J. McGeehin, J. Pallister, M. Regalado, M. Rubin, B. Tubiana Jr., and J. V. Umbal, 1996: Eruptive history of Mount Pinatubo. In: Newhall, C. G. and R. S. Punongbayan (Eds.), *Fire and Mud: Eruptions and Lahars of Mount Pinatubo*, University of Washington Press, Seattle, 165-196.
- Pathier, E., 2003: Apports de l'interferometrie radar differentielle a l'etude de la tectonique active de Taiwan. Ph.D. Thesis, Universite Marne-La-Vallee, Paris, France, 273 pp.
- Pathier, E., B. Fruneau, B. Deffontaines, J. Angelier, C. P. Chang, S. B. Yu, and C. T. Lee, 2003: Coseismic displacements of the footwall of Chelungpu fault by the 1999, Taiwan, Chi-Chi earthquake from InSAR and GPS data. *Earth Planet. Sci. Lett.*, **212**, 73-88.
- Rau, R. J., K. E. Ching, J. C. Hu, and J. C. Lee, 2008: Crustal deformation and block kinematics in transition from collision to subduction: Global positioning system measurements in northern Taiwan, 1995-2005. *J. Geophys. Res.*, **113**, B09404, doi: 10.1029/2007JB005414. [[Link](#)]
- Spence, R. J. S., A. Pomonis, P. J. Baxter, A. W. Coburn, M. White, M. Dayrir, and Fiels Epidemiology Training Program Team, 1996: Building damage caused by the Mount Pinatubo eruption of June 15, 1991. In: Newhall, C. G. and R. S. Punongbayan (Eds.), *Fire and Mud: Eruptions and Lahars of Mount Pinatubo*, University of Washington Press, Seattle, USA, 1055-1062.
- Teng, L. S., 1990: Geotectonic evolution of late Cenozoic arc-continental collision in Taiwan. *Tectonophysics*

- ics*, **183**, 57-76, doi: 10.1016/0040-1951(90)90188-E. [[Link](#)]
- Teng, L. S., W. Yuan, C. H. Tang, C. Y. Huang, T. C. Huang, M. S. Yu, and A. Ke, 1991: Tectonic aspects of the Paleogene depositional basin of northern Taiwan. *Proc. Geol. Soc. China*, **34**, 313-336.
- Teng, L. S., C. T. Lee, C. H. Peng, W. F. Chan, and C. J. Chu, 2001: Origin and geological evolution of the Taipai Basin, northern Taiwan. *West. Pac. Earth Sci.*, **1**, 115-142.
- Tsai, Y. B., 1986: Seismotectonics of Taiwan. *Tectonophysics*, **125**, 17-37, doi: 10.1016/0040-1951(86)90005-3. [[Link](#)]
- Wang, C. S., Y. L. Tsai, and M. L. Ger, 1995: Reflection seismic stratigraphy in Taipei Basin (II)- western and southern Taipei Basin. *J. Geol. Soc. China*, **38**, 141-172.
- Werner, C., U. Wegmuller, T. Strozzi, and A. Wiesmann, 2003: Interferometric point target analysis for deformation mapping. Paper presented at International Geoscience and Remote Sensing Symposium (IGRSS), Toulouse, France.
- Yamashina, K. and H. Shimizu, 1999: Crustal deformation in the mid-May 1991 crisis preceding the extrusion of a dacite lava dome at Unzen volcano, Japan. *J. Volcanol. Geotherm. Res.*, **89**, 43-55, doi: 10.1016/S0377-0273(98)00121-8. [[Link](#)]
- Yeh, Y. H. and K. R. Chen, 1990: unpublished report of research project entitled "Investigation of the Kanchiao Fault- micro-seismic observation", funded by National Science Council.
- Yu, S. B., H. Y. Chen, and L. C. Kuo, 1997: Velocity field of GPS stations in the Taiwan area. *Tectonophysics*, **274**, 41-59, doi: 10.1016/S0040-1951(96)00297-1. [[Link](#)]
- Zebker, H. A., P. A. Rosen, R. M. Goldstein, A. Gabriel, and C. L. Werner, 1994: On the derivation of coseismic displacement fields using differential radar interferometry: The Landers earthquake. *J. Geophys. Res.*, **99**, 19617-19634.